Supplementary Information for

Ordered aqueous structures from liquid-liquid phase separation by supramolecular polymerizations

Hailin Fu[1,2], Jingyi Huang[1,3], Joost J. B. van der Tol[1,2], Lu Su[4], Swayandipta Dey[1,5], Peter Zijlstra[1,5], Ghislaine Vantomme[1,2], Patricia Y. W. Dankers[1,3], E. W. Meijer[1,2,6]**

[1]Institute for Complex Molecular Systems, Eindhoven University of Technology, P.O. Box 513, 5600 MB, Eindhoven, The Netherlands.

[2]Laboratory of Macromolecular and Organic chemistry, Eindhoven University of Technology, P.O. Box 513, 5600 MB, Eindhoven, The Netherlands.

[3]Department of Biomedical Engineering, Eindhoven University of Technology, P.O. Box 513, 5600 MB, Eindhoven, The Netherlands.

[4]Leiden Academic Centre for Drug Research, Leiden University, 2333 CC, Leiden, The Netherlands.

[5]Department of Applied Physics and Eindhoven Hendrik Casimir Institute, Eindhoven University of Technology, P.O. Box 513, 5600 MB, Eindhoven, The Netherlands.

[6]School of Chemistry and RNA Institute, University of New South Wales, Sydney, NSW 2052, Australia.

*Correspondence to: E.W.Meijer@tue.nl; h.fu@tue.nl

Content

Materials

All chemicals and reagents were purchased from commercial sources at the highest purity available and used as received unless otherwise stated. UPy-Gly, BTA-EG_4 and BTA-Glc were obtained from SymoChem. mPEG-O-C12 (DPEG, PEG MW: 5000), PEG-FITC (MW: 10k) and dextran-FITC (MW: 550k) were obtained from Creative PEGWorks. PEG (MW: 8000), cetrimonium bromide (CTAB) and alginate and sodium salt from brown algae were purchased from Sigma-Aldrich. Dextran 500 was ordered from Pharmacosmos (Pharmaceutical quality). Water was purified on an EMD Millipore Milli-Q Integral Water Purification system.

UPy-COOH was synthesized following previous methods[1,2]. The synthesis of BTA-Cy5 is also reported in our previous work[3].

Synthesis of UPy-Cy5

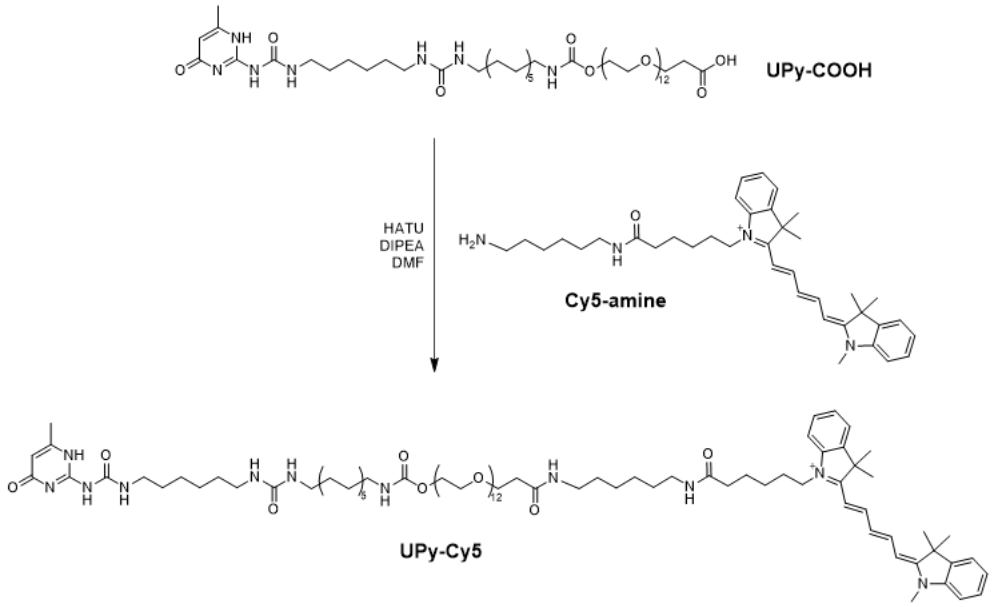

The deprotected UPy-COOH (12 mg; 0.011 mmol) was dissolved in 2 mL of DMF. HATU (5 mg; 0.012 mmol) and DIPEA (9 μL; 0.048 mmol) were then added for pre-activation and the mixture was stirred for five minutes. After that, the Cy5-amine was added (5 mg; 0.0086 mmol) and the reaction was stirred for one hour. The organic phase was then diluted in DCM (10 ml), followed by washing with brine and evaporation of the DCM. The resulting crude was purified by preparative reverse phase LC-MS to yield the desired compound (5.8 mg; 31%). The LC-MS [M] of UPy-Cy5 was calculated 1701.11, found 567.75 $[M+4H]^{4+}$, 851.06 $[M+2H]^{2+}$ and 1701.33 $[M+H]^{+}$.

Sample preparation

UPy-Gly or UPy-COOH stock solution: The stock solution was always freshly made. 4 wt% of stock solution were prepared by dissolving either UPy-Gly or UPy-COOH solid in the PBS buffer and a calculated amount of 1 M NaOH to make the final pH higher than 11. The solution was then heated at 75 °C for 15 min. Subsequently, a calculated amount of 600 μM of UPy-Cy5 or 1 mM of Nile Red in methanol was added and mixed with the stock solution to reach a

final concentration of 7.2 µM (UPy-Cy5) or 2 µM (Nile Red). Finally, 1 M HCl was added to adjust the pH to the targeted pH.

UPy-Gly or UPy-COOH solution with dextran: The freshly made UPy-Gly or UPy-COOH stock solution was immediately added into the pre-diluted PBS solution and mixed. Then 10 or 20 wt% of dextran solution (with 0.08 mol% of dextran-FITC) was added to reach to the required concentration. The mixture was vortexed for at least 20 seconds.

UPy-Gly or UPy-COOH solution with PEG and dextran: The freshly made UPy-Gly or UPy-COOH stock solution was immediately added into the pre-mixed PBS and PEG solution and mixed. 10 or 20 wt% of dextran solution (with 0.08 mol% of dextran-FITC) was then added to achieve the required concentration. The mixture was vortexed for at least 20 seconds.

BTA-EG_4 solution with CTAB: 4 mg/mL of BTA-EG_4 stock solution was freshly made by mixing BTA-EG_4 solid with 0.1 mol equiv. of CTAB and water and stirred and heated at 80 ℃ for 15 min. 500 µM of BTA-Cy5 in methanol was added after heating to get a final concentration of about 1 µM. A small volume of the concentrated CTAB solution (50 mg/mL) was added to adjust the BTA-EG_4/CTAB ratio later.

BTA-Glc solution with PEG and dextran: 4 mg/mL of BTA-Glc stock solution was prepared by dissolving BTA-Glc solid in water and stirred and heated at 75 ℃ for 15 min. 500 µM of BTA-Cy5 in methanol was added after heating to get a final concentration of 1 or 2 µM. The stock solution was then mixed with the heated DPEG solution. Next, the pre-heated 20 wt% of PEG was added before adding 20 wt% of dextran solution (with 0.08 mol% of dextran-FITC). The volumes of the added solutions were adjusted to arrive at the designed concentrations. The solution was shaken or vortexed after each step. All solutions except for the UPy-Gly or UPy-COOH stock solution were either incubated in the Eppendorf tube or transferred to the imaging chambers immediately after the preparation.

Methods

Zeta Potential Measurements

Zeta potentials were measured on a Malvern instrument Zetasizer, model Nano ZSP. Zetasizer software was used to analyze and process the zeta potential data. For the preparation of UPy-COOH and UPy-Gly samples, the solid samples were dissolved and annealed in basic 0.84 x PBS (110 mM NaOH) at a concentration of 4.4 wt% for 15 minutes at 70 °C. After dissolving, the samples were diluted with MiliQ and 1x PBS and adjusted to the final pH varying from 4.6 to 9 with 1 M HCl, resulting in 0.4 mM of UPy-Gly or UPy-COOH with different PBS concentrations. A DTS1070 cuvette was used for measuring the zeta potential. The measurement duration time was automated, and automatic attenuation and voltage was selected. The samples were measured in triplo at RT with a 30 s equilibration time.

Dual Asymmetric Centrifugation

To break down the UPy-Gly fibrils, dual asymmetric centrifugation was performed using a Hettich ZentriMix 380 R equipped with a ZentriMix rotor. Samples were added to 0.2 mL Eppendorf tubes and centrifuged for 60 min with a rotational speed of 2,500 rpm. The samples

were only subjected to the shear forces generated by the dual rotor setup with no milling beads added.

Confocal Laser Scanning Microscopy (CLSM)

Sample preparation method 1: 8 to 9 µL of the fresh sample were loaded into a 120 µm thick chamber with two pieces of # 1.5 cover glass on the top and bottom and an imaging spacer (Grace Bio-Labs SecureSeal imaging spacer, 8 wells, diam. × thickness 9 mm × 0.12 mm) in the middle.

Sample preparation method 2: 45 to 48 µL of the fresh sample were loaded into an 800 µm thick chamber (Grace Bio-Labs SecureSeal hybridization chambers, 8 wells, diam. x depth 9 mm x 0.8 mm, port diam. 1.5 mm) with the # 1.5 cover glass at the bottom. The open ports were sealed after sample loading.

Sample preparation method 3: About 100 µL of the fresh sample were loaded into each well of the ibidi µ-slide (18 wells, No. 1.5H glass bottom, well size 5.7 × 6.1 × 6.8 mm^3) and covered with the lid.

Sample preparation method 4: About 5 µL of the sample were loaded onto the glass holder and covered with the # 1.5 cover glass. The surroundings of the cover glass were sealed with nail polish to reduce evaporation induced drifting or flowing.

The fluorescent images and movies were acquired with the Leica TCS SP8 microscope in the confocal mode with 40x/0.9 (dry), 63x/1.2 (water immersion) and 63x/1.3 (oil immersion) objectives at a resolution of 512 × 512, 1024 × 1024 or 2048 × 2048. The lasers used were 488 nm (for FITC), 552 nm (for Nile Red) and 638 nm (for Cy5). The movies were taken with a time gap of 10 min. The z stack images were collected with a gap of 0.5, 1 or 2 µm.

The bright field images were collected with the Leica TCS SP8 microscope in the BF mode.

The image analysis was conducted with image J or the Leica microscope built-in software (only for some z stack images).

Fluorescence Recovery After Photobleaching (FRAP)

The FRAP was conducted on the Leica TCS SP8 microscope in the confocal mode with a 63x/1.2 (water immersion) NA objective at a resolution of 512 × 512 pixels. The samples were dyed with 1.8 µM of UPy-Cy5. One to three images were taken before bleaching with the imaging power of 0.5% to 1%. Subsequently, selected, circular areas with diameters ranging from 0.6 to 7 µm were bleached for 10 cycles (0.3 to 0.7 seconds per cycle) at 50% of power with the 638 nm laser. The following images were captured with 0.5% to 1% of power every 0.3 to 5 seconds. The whole process was automated with the built-in software. Three or more measurements were conducted for each sample. The fluorescence intensities of the ROIs were extracted by imageJ and normalized with the intensities of the reference area following the equation below.

$$i(t) = \frac{I(t) / R(t)}{I(0) / R(0)} \qquad (1)$$

Where *i(t)* is the normalized fluorescence intensity at time t, *I(t)* and *I(0)* are the fluorescence intensities of the ROI at time t and 0, respectively. *R(t)* and *R(0)* are the fluorescence intensities of the reference area at time t and 0, respectively. The normalized fluorescence recovery curves were then fitted with a first-order exponential equation (Eq. 2) where A is the amplitude of the recovery, τ is the critical recovery time and C is the intercept [4].

$$i(t) = A(1 - e^{-t/\tau}) + C \qquad (2)$$

The half-life of the recovery ($t_{1/2}$) could then be determined by Eq. 3 and the apparent diffusion constant (D_{app}) could be calculated by factoring in the radius of the ROI (ω) following Eq. 4[4,5].

$$t_{1/2} = \ln 2 \times \tau \qquad (3)$$

$$D_{app} = \frac{0.88\omega^2}{4t_{1/2}} \qquad (4)$$

Atomic Force Microscopy (AFM)

Wet samples for force curve measurements: The freshly cleaved mica was first treated with 20 µM of $CaCl_2$ for 20 to 30 min and washed with water for 2 to 3 times. The residual solutions were pipetted away from the mica, eventually leaving a thin layer of water on the top. Next, 1 µL of the sample was evenly added onto the mica by immersing the tip of the pipette into the thin water layer. The mica was then incubated at room temperature for at least half an hour. It was either covered or replenished with water to avoid drying during the incubation time. Finally, about 100 µL of the buffer, which contained the same concentration of dextran and PBS as the sample, were mounted onto the mica right before the measurements.

Dry samples for tapping mode imaging: Samples were first diluted into water with a final concentration of 10 µM. 5 µL of the diluted sample were immediately spin-coated onto a freshly cleaved, 1.0 × 1.0 to 1.5 × 1.5 cm^2 sized mica at 2,000 rpm for 1 min.

In-situ force curve measurements on tactoids: AFM measurements were conducted on a Cypher Environmental Scanner (ES) equipped with a closed gas cell. An active heating and cooling stage was used to actively control the temperature at 20 °C. The measured force curves on the tactoids were recorded in contact mode using a super luminescent diode in order to reduce the signal-to-noise ratio. Spherical PMMA-based CP-CONT-PM probes (Nanotools, spring constant k = 0.2 N/m; r = 750 nm) with a resonance frequency of 30 Hz (~ 7 Hz in PBS buffer) were used for all measurements. The cantilever was thermally calibrated in solution with Blue-Drive using the 'Get Real' function in the Igor Pro software. Force curves were obtained using a slow scan rate of 0.061 Hz over a force distance of ~ 4 µm (velocity 414.11 nm/s) in order to prevent any perturbations in the PBS buffer that could cause the displacing of the tactoids. Furthermore, the trigger point was kept between 10 – 15 nN. After obtaining the force curves, we applied the Hertz model (for spherical AFM tips) in order to extract the Young's modulus of the tactoids (Eq. 5).

$$F = \frac{4}{3} * \frac{E_S}{1 - V_S^2} * \sqrt{\mathrm{r}} * \delta^{\frac{2}{3}} \qquad (5)$$

where F is the applied force, E_s is the Young's modulus, V_s is the Poisson's ratio （V_s = 0.4）, r is the radius of the spherical AFM tip and δ is the indentation depth. For all samples, multiple force curves (6 to 26) were recorded, and mean values and standard deviations were extracted. Two-sample student t tests were performed to verify the difference between two populations.

Tapping mode imaging of fibrils: AFM measurements of dry samples in tapping mode (phase < 90) were similarly recorded on the Cypher Environmental Scanner (ES) equipped with a closed cell and a normal laser diode. A heating and cooling stage was used to actively control the temperature at 20 °C. Silicon AC-160TS probes (Oxford instruments, spring constant k = 26 N/m; f = 300 kHz) with a tip height of 14 µm and a radius of 7 nm were used for all measurements and calibrated using the 'Get Real' function in the Igor Pro software. Either 20 × 20 or 10 × 10 µm height images were acquired using a scan rate of 3.0 Hz and 1024 × 1024 pixels. Contrast of the images was further enhanced using first order planefit and flattening using Gwyddion v2.60. Subsequently, the lengths of the UPy-Gly fibrils in the processed images were measured using the Digimizer software. The histograms of the fibril length were fitted with the Gaussian distributions.

Cryogenic Transmission Electron Microscopy (Cryo TEM)

For cryo-TEM measurements Quantifoil grids (R 2/2, Quantifoil Micro Tools GmbH) or Lacey grids (LC200-Cu, Electron Microscopy Sciences) were used. Prior to sample addition, grids were treated with surface plasma at 5 mA for 40 s using a Cressington 208 carbon coater. 3 µL of the sample were applied to the grid held in an automated vitrification robot (FEI Vitrobot™ Mark IV), operating at 22 °C with a relative humidity of 100%. Excess sample was removed by blotting for 3 s using the filter paper with a blotting force of -2. The thin film formed was vitrified by plunging the grid into liquid ethane just above its freezing point. Vitrified films were transferred into the vacuum of a CryoTITAN (Thermo Fihser) equipped with a field emission gun that was operated at 300 kV, a post-column Gatan energy filter, and a 2048 × 2048 Gatan CCD camera. Virtrified films were observed in the CryoTITAN microscope at temperatures below −170°C. Micrographs were taken at low dose conditions, using defocus values including -10 µm, -5 µm and -2.5 µm at 24k magnification.

The fibril diameters were extracted from multiple cryo TEM images per sample with imageJ. The histograms of the fibril diameters could be fitted with the Gaussion distribution. Two-sample t tests were carried out to verify the difference of mean values between two populations.

Polarized Fluorescence Microscopy

Sample preparation: 2 µL of the sample were added onto the holding glass and covered with #1.5 cover glass. The sides of the cover glass were sealed with the nail polish to avoid evaporation and sample drifting.

Optical polarization measurements: The samples were imaged using a commercially available inverted microscope (model: Nikon Eclipse Ti2). After the samples were loaded on the microscope stage, it was illuminated (in epi-illumination mode) using a 637 nm excitation laser (OBIS FP 637LX, Coherent). The excitation parameters (excitation power 0.1 mW) were controlled using the Coherent software. The collimated laser beam was first allowed to pass

through a 640 ± 10 nm bandpass filter, followed by a zero-order half-wave plate (Thorlabs) which is mounted on a rotation mount. The excitation beam was reflected by a dichroic mirror (ZT640rdc, Chroma) and was directed to an oil-immersion objective (Apo-TIRF, 60x, 1.49 NA, Nikon). This setup results in the sample being illuminated with a collimated light-beam with a well-controlled polarization state. To eliminate the concern of the depolarization of the excited light passing through the optics, we mounted a polarizer on top of the objective lens and measured the laser intensity by tuning the angle of the half wave plate. The minimum laser intensity detected was almost zero. This suggests almost 100% of polarization of the excited light.

The fluorescence signal was collected by the same objective lens and passed through a 635 nm notch filter and a 700 ± 75 nm bandpass filter before being collected by the detector (Prime BSI Express sCMOS camera, Teledyne Photometrics). The widefield fluorescence images from the samples were captured using NIS Elements (Nikon) with an exposure time of 100 ms. For each sample, multiple 225 s or longer movies were recorded with the halfwave plate manually rotated by 4 degrees every 5 s. This resulted in a polarization rotation of 2θ when the halfwave plate was rotated by θ.

The fluorescence intensities of the tactoids were extracted using imageJ and plotted against the polarization angle of the incident light beam (Fig. 3g and Supplementary Fig. 8). To fit the oscillating fluorescence intensity curves, we first studied the bleaching effect and found that the intensities decayed linearly over time and that the bleaching rate was roughly linear to the starting intensity (Supplementary Fig. 6). Subsequently, we modified the squared cosine function and fitted the oscillatory curves with the following equations using Origin.

$$I(\theta) = (I_0 - kt)\cos^2(\theta + \theta_0) + b(1 - kt / I_0) \tag{6}$$

$$t = \frac{5\theta}{8} \tag{7}$$

Where I_0 is the amplitude of the oscillation curve and b is a constant that is not sensitive to the angle of the linearly polarized light (θ). k is the decaying rate of the amplitude due to bleaching. θ_0 is related to the orientation of the dyes. The extent of alignment (α) of the fibrils within the tactoids can thus be calculated by Eq. 8.

$$\alpha = \frac{I_0}{I_0 + b} \tag{8}$$

The good correlation between the angles of the dyes (θ_0) and the relative orientations of the tactoids ($\theta_{tactoids}$) obtained from the images confirmed correlated positioning between the dyes and the fibrils (Supplementary Fig. 7).

Small Angle X ray Scattering (SAXS)

The SAXS measurements were conducted on a SAXSLAB Ganesha system, equipped with a GeniX-Cu ultra-low divergence source and a photon flux of 1×10^8 photons/s. The wavelength of the X ray is 1.5 Å. About 150 µL of solutions were loaded into each fixed, 2 mm quartz capillary. 2D intensity images were collected with a Pilatus 300K silicon pixel detector with a

measurement of 4 hours and converted to 1D plot with SAXSGUI. The q range covered by a single measurement was 0.12 – 6.9 nm^{-1} and the absolute q value was calibrated with AgBeh. Solvent and capillary contributions to the scattering intensities were subtracted from the blank solution with the PRIMUS program from the ATSAS software package.

Theory

Flory-Huggins Solution Theory

$$f_{Mix} = \frac{\varphi}{N}\ln\varphi + (1-\varphi)\ln(1-\varphi) + \chi\varphi(1-\varphi) \quad (9)$$

The Flory-Huggins mixing free energy per unit volume, for a polymer with a degree of polymerization N, can be written in the dimensionless form above (Eqn. 9), where φ is the volume fraction of the polymer (0 < φ <1) and χ is the polymer-solvent interaction parameter. The first two terms represent the entropy. and the last term stands for the enthalpy. To have phase separation, f_{Mix} is supposed to be positive. Since the entropic terms are negative, χ must be a positive value, suggesting that UPy-Gly supramolecular polymers and water have repulsive interactions. For reference, χ between PEG and water is ~0.3[6]. For a small χ, the sign of f_{Mix} could be switched from negative to positive with the increase of N or the elongation of supramolecular polymers, which means a transition from a stable solution to a metastable or unstable solution. In the metastable state (binodal region), the phase separation proceeds through the nucleation and growth pathway. In the unstable state (spinodal region), the solution would undergo spinodal decomposition. The slow growth of the tactoids especially at relatively low dextran concentrations (Extended Data Fig. 4) suggests a nucleation and growth pathway or a metastable state of the solution.

Macromolecular crowder effect on the phase separation

$$f_{Mix} = \frac{\varphi_1}{N_1}\ln\varphi_1 + \frac{\varphi_2}{N_2}\ln\varphi_2 + \varphi_s\ln\varphi_s + \chi_{12}\varphi_1\varphi_2 + \chi_{1s}\varphi_1\varphi_s + \chi_{2s}\varphi_2\varphi_s \quad (10)$$

Based on the Flory-Huggins solution theory, the mixing free energy per unit volume, for two polymers with degrees of polymerization as N_1 and N_2, can be written in the dimensionless form above (Eqn. 10), where $\varphi_1, \varphi_2, \varphi_s$ are the volume fractions of polymer 1, polymer 2 and the solvent ($\varphi_1 + \varphi_2 + \varphi_s = 1$). $\chi_{12}, \chi_{1s}, \chi_{2s}$ are the interaction parameters of polymer 1/polymer 2, polymer 1/solvent and polymer 2/solvent, respectively[7]. For dextran, its interaction parameter with water is ~0.5 (χ_{2s}) at 25 °C[8]. Since UPy-Gly supramolecular polymers and dextran could phase separate from each other, χ_{12} is also supposed to be positive. When the dextran concentration ($\varphi_2 \ll 1$) is increased, f_{Mix} would also increase. This means that a smaller N_1 could also make f_{Mix} positive or that the phase separation of supramolecular polymers could occur with shorter fibril lengths in the presence of higher concentrations of dextran ($\varphi_1 \ll 1, \varphi_2 \ll 1$). Based on the tactoids of amyloid fibrils, the longer the fibril length, the higher the axial ratio. The decrease of axial ratios above 0.9 wt% of dextran could be related to the enhanced phase separation tendency at shorter fibril lengths. At 3 wt% of dextran and above, the solution turned turbid immediately after mixing, similar to spinodal decomposition.

LLPS of UPy-COOH and BTA-EG$_4$

Similar to UPy-Gly, UPy-COOH supramolecular polymers could also undergo LLPS and form into tactoids, whose shapes and sizes could be controlled by the dextran concentration (Extended Data Fig. 9b). BTA-EG$_4$, however, needs to be coupled with a charged surfactant to induce the formation of tactoids (Extended Data Fig. 9a). The surfactant can be inserted into the supramolecular polymer chains by hydrophobic interactions as reported by our previous work[9]. The charges introduced by the surfactants could reduce fibril entanglement and increase the fibril mobility for easier LLPS. But too many surfactants would make the fibrils too short and/or too repulsive to each other to phase separate.

Continuous and discrete networks of UPy-Gly and UPy-COOH supramolecular polymers

Both UPy-Gly and UPy-COOH are charged, and their zeta potentials are dependent on the pH and salt concentrations (Supplementary Fig. 4). When 5 wt% of PEG or dextran was introduced into the solution of UPy-COOH supramolecular polymers (50 μM), clear difference could be seen using CLSM at different PBS concentrations and pH (Supplementary Fig. 14-15). The aggregation tendency increased at higher PBS concentrations and lower pH due to reduced repulsive interactions. Similarly, in the phase separated solution of PEG and dextran, the supramolecular polymers stayed liquid like at relatively high pH and/or low salt concentrations, which would first undergo LLPS at the liquid-liquid interface and eventually form into a continuous network. At low pH and/or high salt concentrations, the supramolecular polymers turned into rigid rods almost immediately in the PEG/dextran solution and formed into discrete networks that supported or deformed the droplets.

Supplementary Figures

Supplementary Fig. 1:

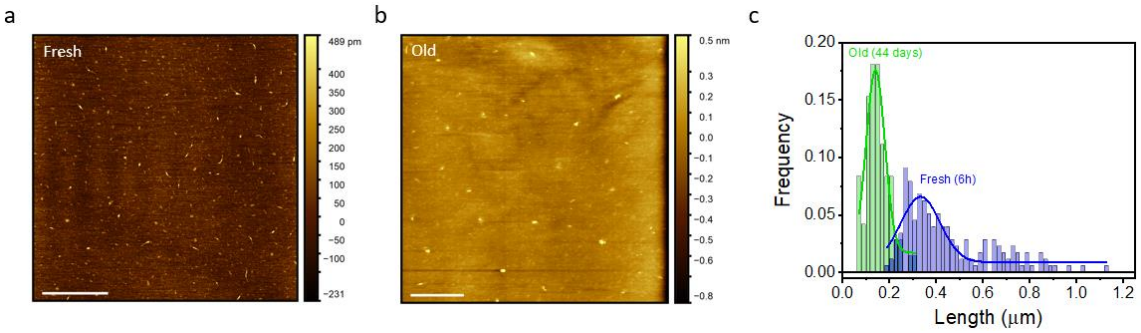

Supplementary Fig. 1 | Comparison of the fresh and old UPy-Gly fibrils at 6 hours after being broken. a, Representative AFM image for fresh fibrils (6 hours old). The scale bar is 4 μm. b, Representative AFM image for old fibrils (44 days old). The scale bar is 2 μm. c, Histograms of the fresh and old fibril lengths 6 hours after being broken. n = 177 (fresh) and 72 (old). The average lengths are 0.45 and 0.15 um for fresh and old fibrils, respectively. This suggests that fresh fibrils grew faster than old ones if we assume similar length distributions for fresh and old samples right after the shearing. UPy-Gly 1 wt% (8.4 mM), pH = 7.6, PBS x 0.25.

Supplementary Fig. 2

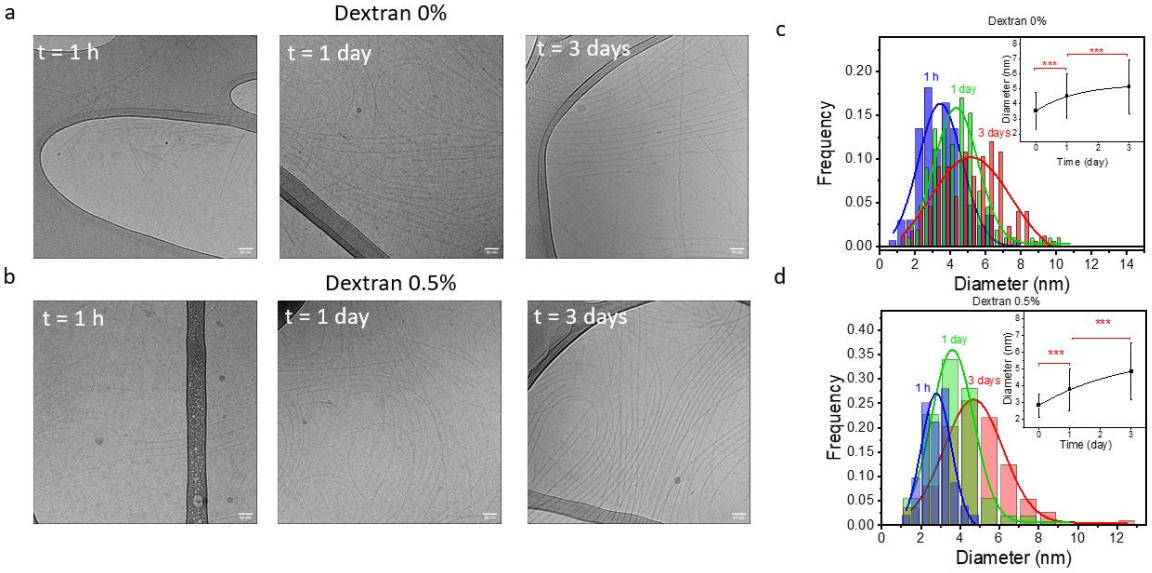

Supplementary Fig. 2 | Tracking the change of fibril diameters with Cryo TEM. a-b, Representative cryo TEM images for the solution with 0 wt% (a) and 0.5 wt% (b) of dextran. The scale bar is 50 nm. c-d, Histograms of the fibril diameter distributions at t = 1 h, 1 day and 3 days for the samples with 0 wt% of dextran (c), n = 112 to 176 and 0.5 wt% of dextran (d), n = 104 to 168. Other solution conditions: UPy-Gly 1 wt%, pH = 7.6, PBS x 0.25. ***: $p < 0.01$.

Supplementary Fig. 3

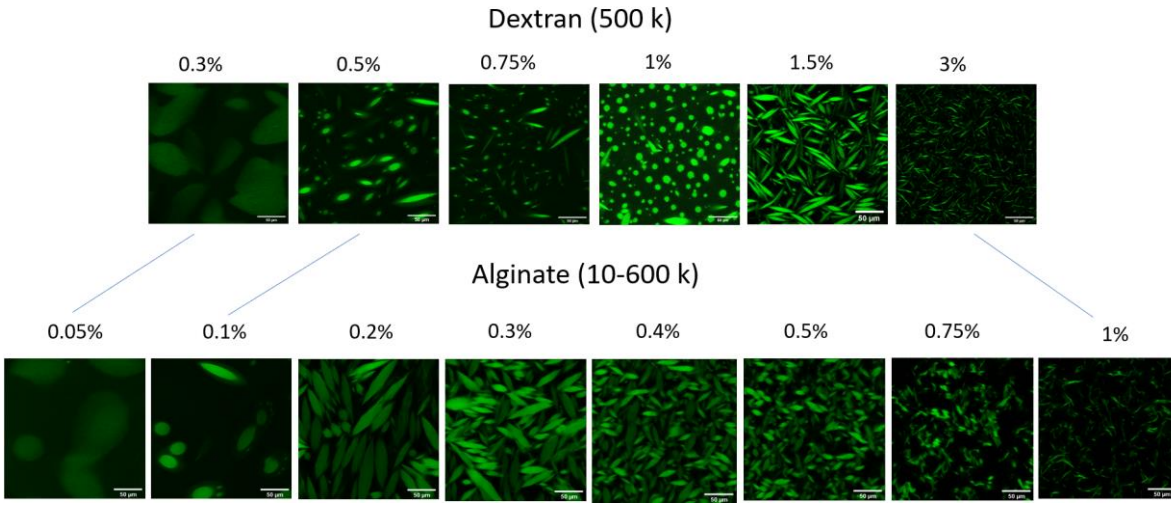

Supplementary Fig. 3 | Comparison of the exclusion effect of dextran and alginate in the LLPS of UPy-Gly supramolecular polymers. Top panel: UPy-Gly solutions with different concentrations of dextran. Bottom panel: UPy-Gly solutions with different concentrations of alginate. All the percentages listed in the image referred to weight percentages. Solution condition: UPy-Gly 1 wt%, pH = 7.6 or 7.7, PBS x 0.25.

Supplementary Fig. 4

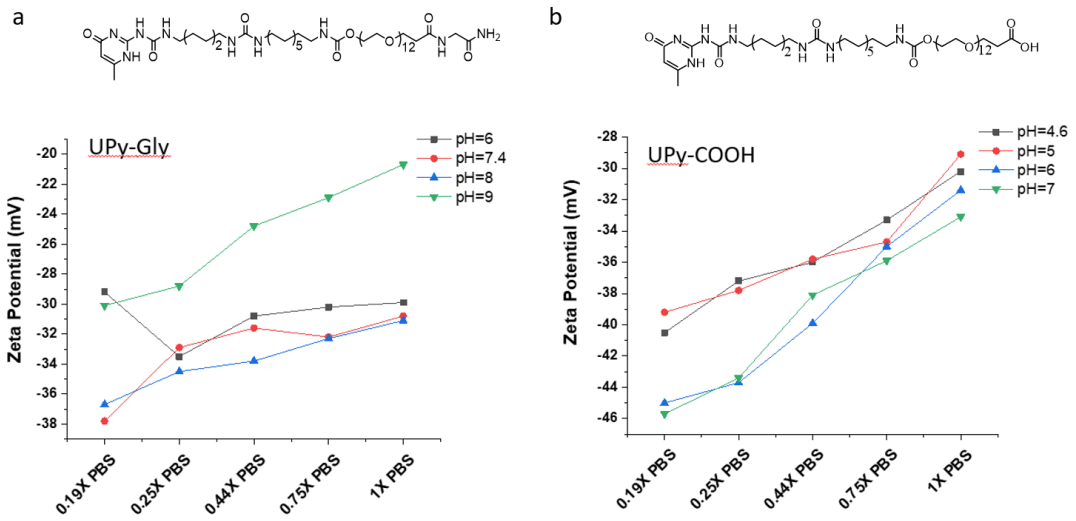

Supplementary Fig. 4 | Zeta potentials of UPy-Gly (a) and UPy-COOH (b) as a function of pH and PBS concentrations.

Supplementary Fig. 5

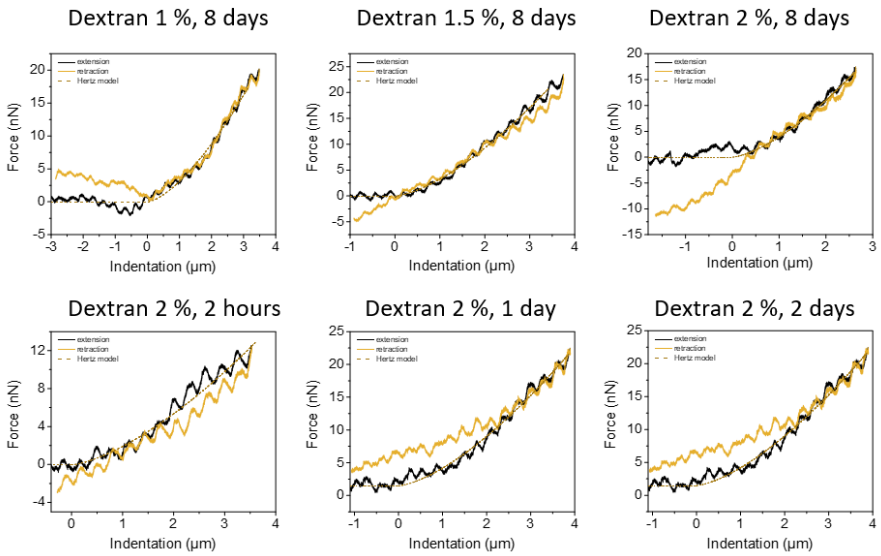

Supplementary Fig. 5 | Representative AFM force curves for tactoids with different ages and different dextran concentrations. Black line: extension curve, yellow line: retraction curve, dashed line: fitted lines of the extension curves with Hertz model. Solution condition: UPy-Gly 1 wt%, pH = 7.6, PBS x 0.25, Dextran 1 wt%, 1.5 wt% and 2 wt%.

Supplementary Fig. 6

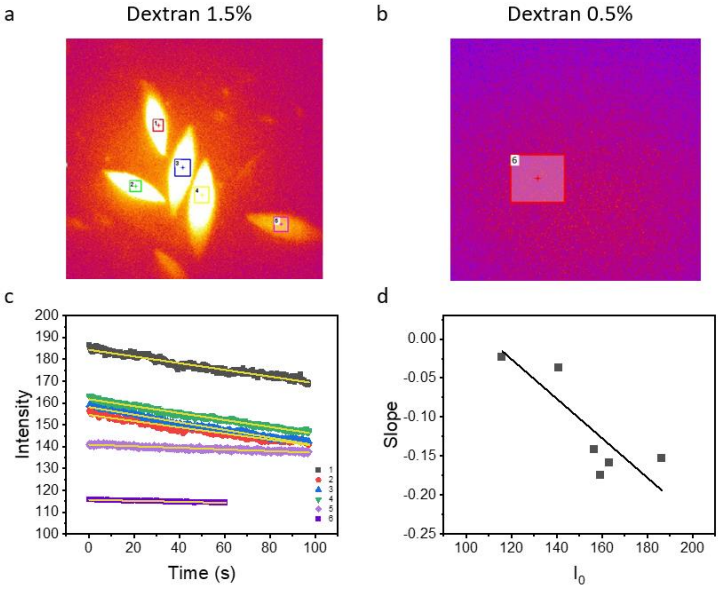

Supplementary Fig. 6 | Linearly decaying fluorescence intensities due to bleaching. a-b, Representative images from polarized fluorescence microscope for solutions with 1.5 wt% of dextran after phase separation (a) and 0.5 wt% of dextran before phase separation (b). Solution condition: UPy-Gly 1 wt%, pH = 7.6, PBS x 0.25. c, Plot of fluorescence intensities over time for the selected areas in a and b. d, Plot of the fluorescence intensity decaying slopes against the starting intensity at the selected areas in a and b.

Supplementary Fig. 7

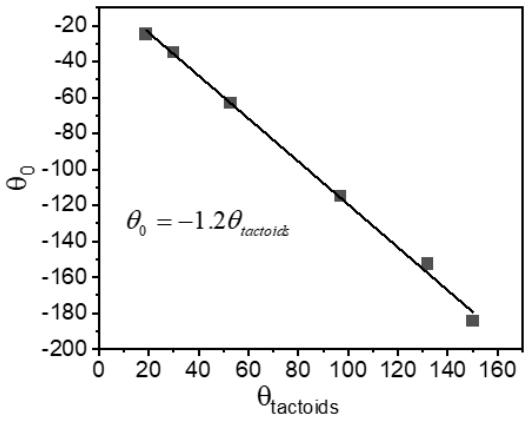

Supplementary Fig. 7 | Plot of the relative angle of the dyes (θ_0) against the angle of the tactoids ($\theta_{tactoids}$). Solution condition: UPy-Gly 1 wt%, Dextran 1 wt%, pH = 7.5, PBS x 0.25, 1 day old.

Supplementary Fig. 8

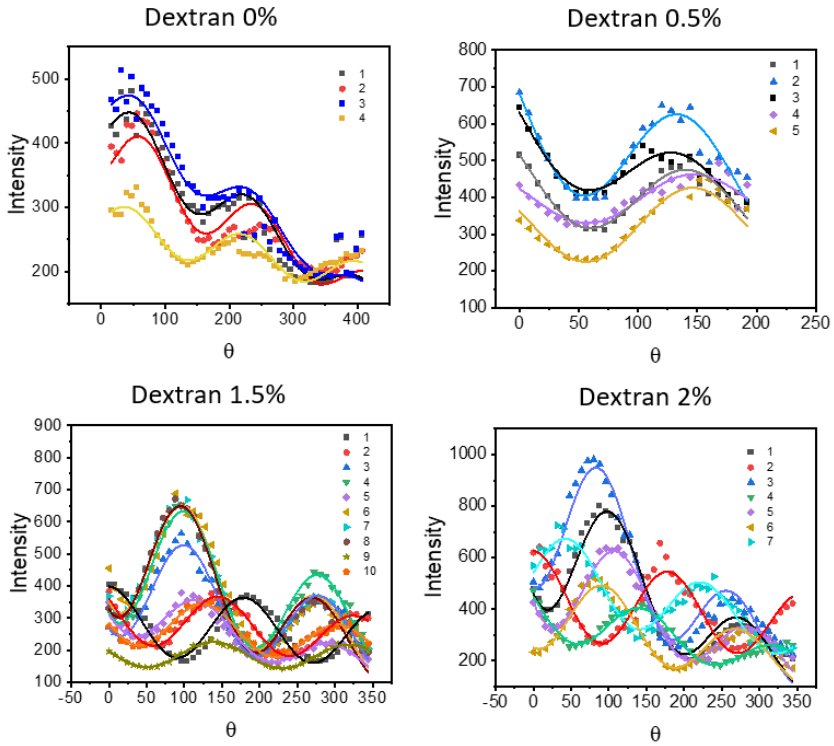

Supplementary Fig. 8 | Polarised fluorescence microscope image analysis for tactoids in the presence of different concentrations of dextran. Example fluorescence intensity oscillation curves and fitted lines. The numbers in the legends refer to different positions on the tactoids. Solution condition: UPy-Gly 1 wt%, Dextran: 0 wt%, 0.5 wt%, 1.5 wt% and 2 wt%, pH = 7.5, PBS x 0.25, 2 days old.

Supplementary Fig. 9

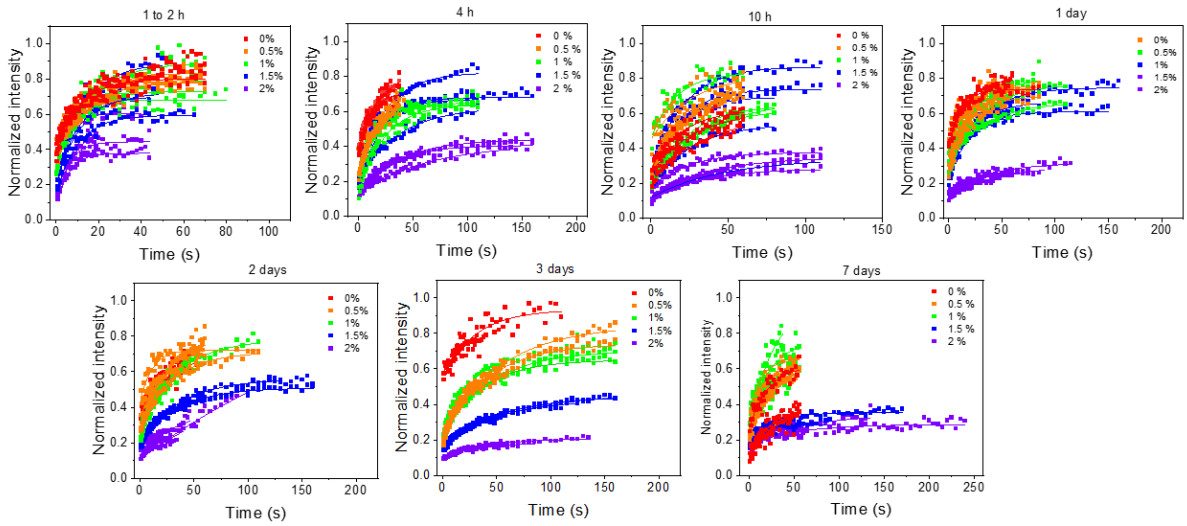

Supplementary Fig. 9 | FRAP curves and fitted lines for different solutions at different time. Solution condition: UPy-Gly 1 wt%, Dextran: 0 wt%, 0.5 wt%, 1 wt%, 1.5 wt%, 2 wt%, pH = 7.6, PBS x 0.25. Time: 1 to 2 hours, 4 hours, 10 hours, 1 day, 2 days, 3 days, and 7 days.

Supplementary Fig. 10

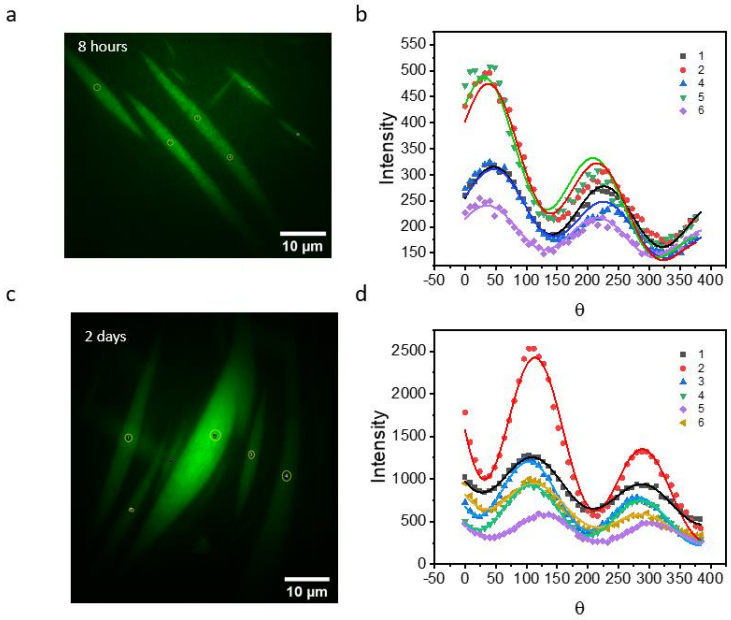

Supplementary Fig. 10 | Polarised fluorescence microscope image analysis for tactoids at different time. a, Representative image for 8 hours old of tactoids. b, Fitting of the fluorescence intensity oscillation curves extracted from a. c, Representative image for the 2 days old tactoids. d, Fitting of the fluorescence intensity oscillation curves extracted from c. Solution condition: UPy-Gly 1 wt%, Dextran 1 wt%, pH = 7.5, PBS x 0.25.

Supplementary Fig. 11

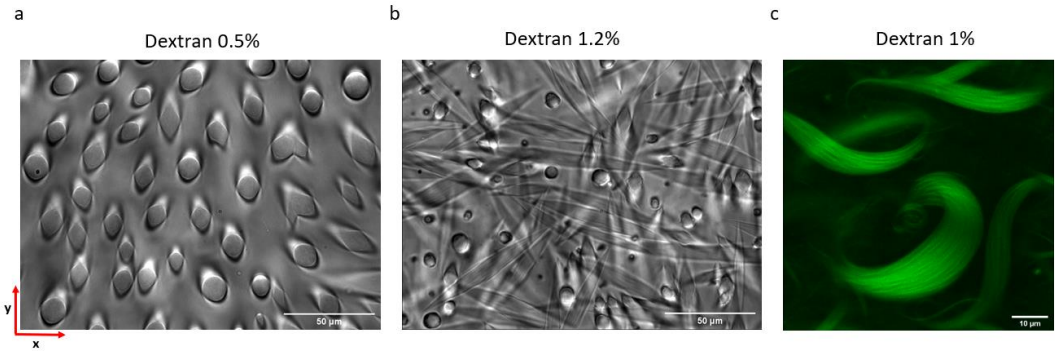

Supplementary Fig. 11 | Bundling of fibrils within the tactoids. a-b, Tactoids visualized by bright field imaging at the x-y plane with 0.5 wt% (a) and 1.2 wt% (b) of dextran. c, Confocal image of tactoids with 1 wt% of dextran (1 month old). The tactoids were treated with acetone through slow solvent exchange. Solution condition: UPy-Gly 1 wt%, pH = 7.6, PBS x 0.25.

Supplementary Fig. 12

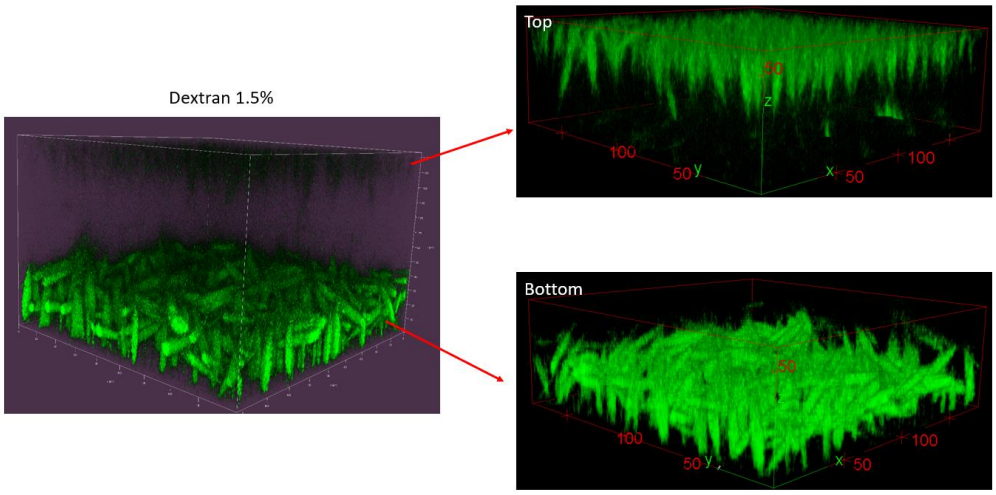

Supplementary Fig. 12 | 3D images of tactoids with 1.5 wt% of dextran. Solution condition: UPy-Gly 1 wt%, Dextran 1.5 wt%, pH = 7.6, PBS x 0.25, 14 days. The sample was incubated in a 120 µm thick chamber with one piece of glass on the top and at the bottom each. The unit of the xyz axis is µm.

Supplementary Fig. 13

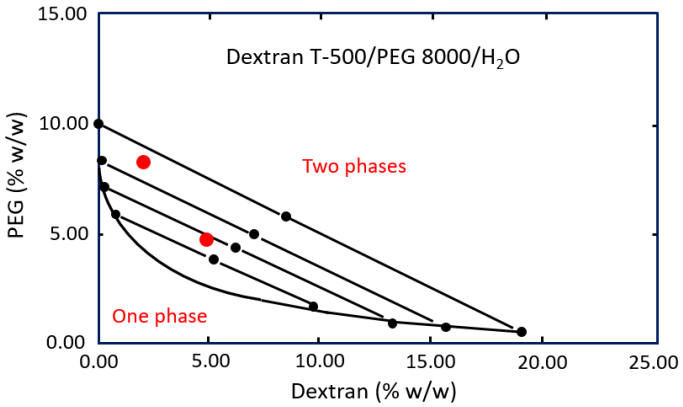

Supplementary Fig. 13 | Phase diagram of PEG (8 kDa) and dextran (T-500) in aqueous solution[10]**.** The red dots represent the compositions used in this paper, which are 5 wt% PEG/ 5 wt% dextran and 8 wt% PEG /2 wt% dextran.

Supplementary Fig. 14

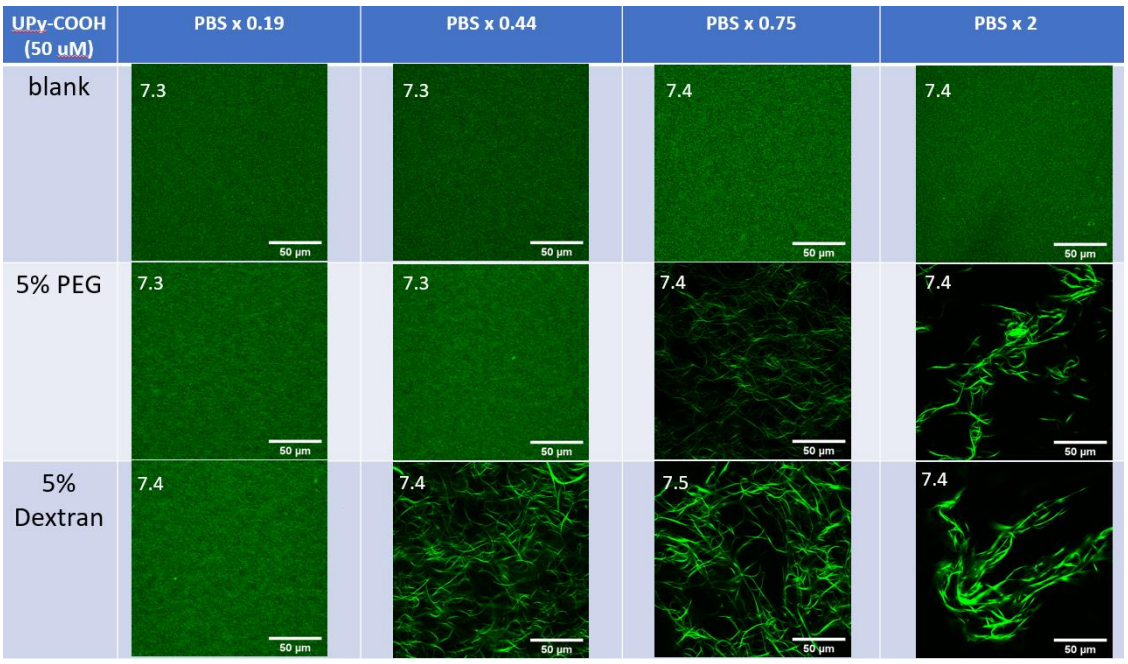

Supplementary Fig. 14 | Salt effect on the aggregation of UPy-COOH supramolecular polymers. Solution conditions: UPy-COOH 50 µM, pH = 7.3 to 7.5, PBS x 0.19, 0.44, 0.75, 2. Top row: blank, middle row: + 5 wt% of PEG, bottom row: + 5 wt% of dextran.

Supplementary Fig. 15

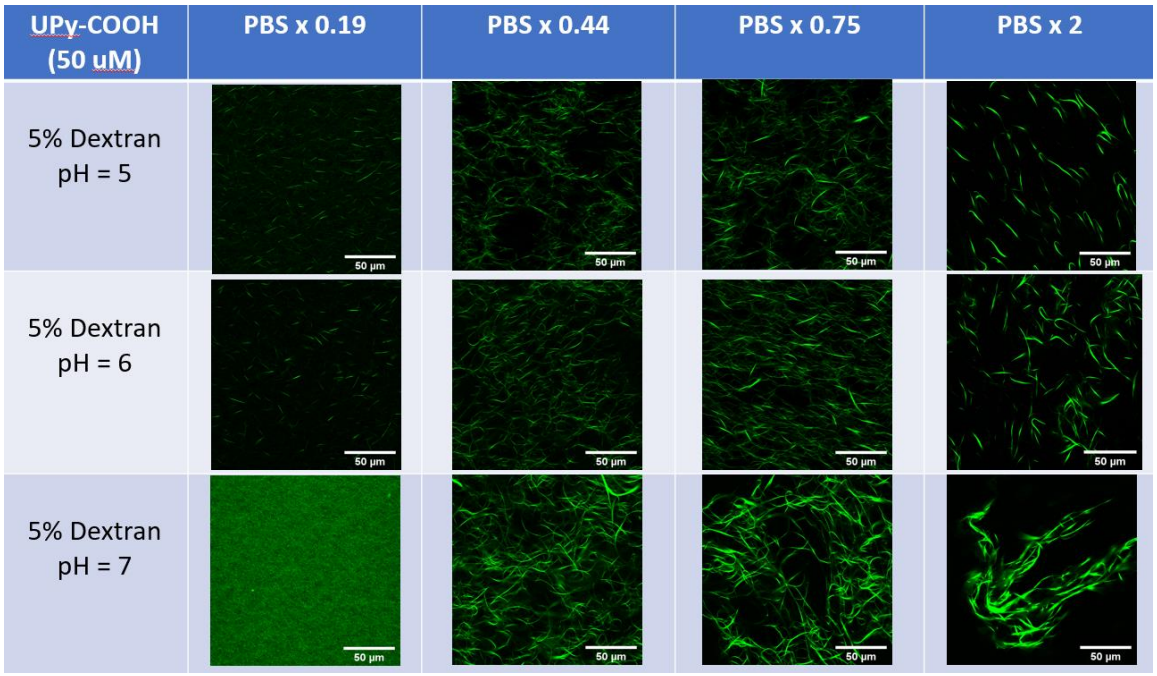

Supplementary Fig. 15 | pH effect on the aggregation of UPy-COOH supramolecular polymers. Solution conditions: UPy-COOH 50 µM, 5 wt% of dextran, pH =5, 6, 7, PBS x 0.19, 0.44, 0.75, 2.

References

1. De Feijter, I. *et al.* Solid-phase-based synthesis of ureidopyrimidinone-peptide conjugates for supramolecular biomaterials. *Synlett.* **26**, 2707-2713 (2015).

2. Dankers, P. Y. W., *et al*. Convenient solid-phase synthesis of ureido-pyrimidinone modified peptides. *Eur. J. Org. Chem.* **22**, 3622–3632 (2007).

3. Baker, M. B. *et al.* Consequences of chirality on the dynamics of a water-soluble supramolecular polymer. *Nat. Commun.* **6**, 6234 (2015).

4. Yewdall, N. A. *et al.* Physicochemical Characterization of Polymer-Stabilized Coacervate Protocells. *ChemBioChem.* **20**, 2643-2652 (2019).

5. Poudyal, R. R. *et al.* Template-directed RNA polymerization and enhanced ribozyme catalysis inside membraneless compartments formed by coacervates. *Nat. Commun.* **10**, 490 (2019).

6. Bae, Y. C., Shim, J. J., Soane, D. S. & Prausnitz, J. M. Representation of vapor–liquid and liquid–liquid equilibria for binary systems containing polymers: Applicability of an extended flory–huggins equation. *J. Appl. Polym. Sci.* **47**, 1193-1206 (1993).

7. Shrinivas, K. & Brenner, M. P. Phase separation in fluids with many interacting components. *Proc. Natl. Acad. Sci. USA* **118**, e2108551118 (2021).

8. Bercea, M., Nichifor, M., Eckelt, J. & Wolf, B. A. Dextran-Based polycations: Thermodynamic interaction with water as compared with unsubstituted dextran, 2-flory/huggins interaction parameter. *Macromol. Chem. Phys.* **212**, 1932-1940 (2011).

9. Su, L. *et al.* Dilution-induced gel-sol-gel-sol transitions by competitive supramolecular pathways in water. *Science* **377**, 213–218 (2022).

10. Diamond, A. D. & Hsu, J. T. Phase diagrams for dextran-PEG aqueous two-phase systems at 22°C. *Biotechnology Techniques* **3**, 119-124 (1989).